IIETA International Information and Engineering Technology Association
Advancing the World of Information and Engineering

Revue des Composites et des Matériaux Avancés-Journal of Composite and Advanced Materials
Vol. 36, No. 2, April, 2026, pp. 243-255
Journal homepage: http://iieta.org/journals/rcma

Optimization of Fused Deposition Modeling Parameters for Tensile Performance of Thermoplastic Polyurethane via Taguchi-Analysis of Variance Analysis

Van Viet Ma[1], Cuong Tran Cong Viet[2], Huu Nghi Huynh[2*]

[1] Faculty of Mechanical Technology, Ho Chi Minh City University of Industry and Trade (HUIT), Ho Chi Minh City 700000, Vietnam
[2] Faculty of Mechanical Engineering, Ho Chi Minh City University of Technology (HCMUT), Ho Chi Minh City 700000, Vietnam

Corresponding Author Email: hhnghi@hcmut.edu.vn

https://doi.org/10.18280/rcma.360203

Received: 17 January 2026
Revised: 11 March 2026
Accepted: 20 March 2026
Available online: 30 April 2026

Keywords:
thermoplastic polyurethane, fused deposition modeling, Taguchi method, 3D printing, tensile strength, analysis of variance

ABSTRACT

Additive manufacturing (AM) has been widely adopted across engineering and biomedical applications, with thermoplastic polyurethane (TPU) emerging as a promising material for fused deposition modeling (FDM) due to its high elasticity and abrasion resistance. However, the mechanical performance of TPU components is highly sensitive to processing conditions. This study systematically investigates the effects of four key FDM parameters-printing temperature, printing speed, layer height, and infill pattern-on the tensile behavior of TPU using a Taguchi L9 orthogonal array combined with analysis of variance (ANOVA). The optimal parameter combination was identified as a printing temperature of 210 ℃, printing speed of 40 mm/s, layer height of 0.16 mm, and a grid infill pattern. Under these conditions, a tensile strength of 21.92 MPa was achieved, accompanied by an enhanced elongation at break. Compared to the baseline parameter set, this represents a significant improvement in tensile performance, highlighting the effectiveness of parameter optimization in strengthening interlayer bonding and load transfer efficiency. ANOVA results indicate that printing temperature is the dominant factor governing all mechanical responses, contributing up to 76.5% of the variation in stiffness, while infill pattern plays a critical role in controlling elongation behavior. Scanning electron microscopy (SEM) reveals improved filament fusion and a more ductile fracture morphology under optimized conditions, confirming the microstructural origin of the enhanced mechanical properties. These findings demonstrate that strategic control of processing parameters can substantially improve both the strength and ductility of FDM-printed TPU, providing practical guidelines for the design of high-performance flexible components.

1. INTRODUCTION

Additive manufacturing (AM), commonly referred to as 3D printing, comprises more than 30 related technologies and has experienced rapid expansion across a wide range of application domains, including food processing, healthcare, education, consumer and household products, as well as high-performance sectors such as automotive engineering, aerospace, security, and defense. Among these technologies, fused deposition modeling (FDM) has become one of the most widely adopted methods due to its relatively low cost, ease of implementation, and broad material compatibility. As a result, numerous studies have investigated the application of FDM in diverse fields, including biomedical material development and testing [1-3], medical device manufacturing [4], aerodynamic drag reduction [5], aircraft and unmanned aerial vehicle components [6], gearbox development [7], and construction applications [8, 9].

In many of these applications, mechanical performance-particularly tensile behavior-plays a critical role in determining the functionality, durability, and reliability of printed components. Tensile strength and elongation are especially important for parts subjected to continuous tensile and deformation loads, such as flexible transmission elements and airless tire structures fabricated using elastomeric materials like thermoplastic polyurethane (TPU) [10]. Consequently, understanding and optimizing tensile mechanical properties have become a central topic in FDM research.

Tensile strength in FDM is governed by interlayer bonding quality, material flow behavior, and internal structural continuity, all of which are directly influenced by printing parameters. Consequently, extensive research has been conducted to identify the dominant parameters affecting tensile performance across different thermoplastic materials. Although the specific influence of individual parameters

varies with material type, several consistent trends can be identified.

Across rigid thermoplastics such as Acrylonitrile Butadiene Styrene (ABS) and Polyethylene Terephthalate Glycol-modified (PETG), infill density and layer height consistently emerge as the primary determinants of tensile strength. Studies by Gupta et al. [11] demonstrated that increasing layer height reduces tensile strength due to weakened interlayer adhesion, while higher infill densities enhance tensile strength by improving internal load transfer. Notably, printing speed exhibits negligible influence on tensile strength for these materials, suggesting that within typical processing ranges, mechanical performance is more strongly governed by geometric and structural factors than by deposition rate.

For Polylactic Acid (PLA), which has been the most extensively studied FDM material, the dominance of infill density and layer height is even more pronounced. Multiple studies indicate that high infill density maximizes tensile strength by reducing internal voids and enhancing stress distribution. Ekşi and Karakaya [12] confirm that infill density is the most influential parameter, followed by layer height and layer width, while printing speed plays a secondary role. This hierarchy reflects the fact that tensile failure in PLA specimens is largely controlled by interlayer bonding area and internal porosity rather than by extrusion dynamics alone.

However, the influence of thermal parameters and printing speed becomes more significant when infill orientation is considered. Sapkota et al. [13] showed that at higher infill angles (e.g., 90°), extruder temperature dominates tensile behavior by directly affecting polymer chain diffusion and layer fusion. In contrast, at lower infill angles (0°), layer height becomes the most critical parameter, as load is primarily carried along filament deposition paths. These findings indicate that the mechanical response of FDM parts is highly anisotropic and that parameter significance is strongly dependent on filament orientation relative to the loading direction.

Thermal effects are further emphasized in the work of Trinh et al. [14], who reported that increasing extruder temperature generally enhances tensile strength by improving interlayer bonding, particularly at higher printing speeds. Nevertheless, excessive printing speed and increased layer height reduce tensile strength due to insufficient bonding time and reduced contact area between layers. Bed temperature also contributes positively by reducing thermal gradients and residual stresses, although its influence is secondary compared to extruder temperature and layer height. These results highlight the coupled nature of thermal and geometric parameters in determining tensile performance.

The role of internal structure has also been widely investigated. Studies on infill type and infill ratio [14-18] consistently indicate that tensile strength increases with infill ratio, while the influence of infill type becomes negligible at 100% infill. Concentric and hexagonal infill patterns frequently outperform other geometries due to a more uniform stress distribution. Across these studies, layer height remains a dominant factor, with increased layer height leading to a systematic reduction in tensile strength. Printing speed, in contrast, shows inconsistent influence, further supporting the conclusion that its effect is material- and structure-dependent rather than universal.

Compared with PLA, PETG has received less attention despite its favorable mechanical and thermal properties. Existing studies [19-21] suggest that tensile strength in PETG is sensitive to infill orientation, layer height, and printing speed, while extruder and bed temperatures exert weaker or non-monotonic effects. Several studies report optimal tensile strength at moderate extrusion temperatures and low printing speeds, indicating a trade-off between improved interlayer diffusion and thermal degradation. As with PLA, increasing the infill ratio consistently enhances tensile performance, reinforcing the importance of internal structural continuity.

In contrast to rigid thermoplastics, TPU exhibits fundamentally different behavior due to its high flexibility and low elastic modulus. TPU printing requires direct-drive extrusion systems to avoid filament buckling and compression, which complicates parameter optimization. Unlike PLA or PETG, TPU must be printed at relatively low speeds and elevated extrusion temperatures to ensure stable material flow and sufficient interlayer bonding. These constraints significantly limit the applicable processing window and increase sensitivity to parameter variations. Despite its growing industrial relevance, systematic studies on TPU tensile optimization-particularly those employing statistically designed experiments-remain limited.

The limited number of existing TPU studies indicates that its tensile behavior is governed by mechanisms distinct from those of rigid polymers. Hohimer et al. [22] reported that TPU tensile strength decreases as the infill angle increases from 0° to 90°, indicating a strong dependence on filament orientation relative to the loading direction. Their results also showed a reduction in tensile strength with increasing extrusion temperature, suggesting that excessive thermal input may degrade interlayer bonding in flexible polymers. Similarly, Le et al. [23] identified infill angle as the most influential parameter affecting TPU tensile strength, followed by extrusion temperature, layer height, and infill ratio. This parameter hierarchy contrasts sharply with findings for PLA and PETG, where infill ratio and layer height typically dominate tensile performance. Such discrepancies highlight the fundamentally different deformation and failure mechanisms of TPU and underscore the need for material-specific optimization strategies.

Moreover, existing TPU studies have largely focused on a limited set of parameters, primarily infill angle and extrusion temperature. The roles of other critical input variables-such as printing speed and infill type-have not been systematically investigated, despite their proven influence on tensile strength, elongation, and secant modulus at 100% strain in rigid thermoplastics. Given the viscoelastic nature of TPU, printing speed may significantly affect filament stretching, bonding time, and interlayer diffusion, while infill type may alter load transfer and deformation modes under tensile loading. The absence of comprehensive studies addressing these parameters represents a clear gap in the current literature.

Therefore, this study aims to systematically evaluate the effects of printing temperature, speed, infill type, and layer height on the tensile properties (strength, elongation, and secant modulus at 100% strain) of TPU. A structured experimental approach based on the Taguchi method with an L9 orthogonal array is employed to identify the optimal parameter combinations, while analysis of variance (ANOVA) is used to quantify the relative significance of each parameter. In addition, scanning electron microscopy (SEM) is utilized to examine microstructural differences resulting from variations in printing temperature and speed, thereby providing a mechanistic interpretation of the observed tensile behavior.

2. DESIGN OF EXPERIMENTS

This study employs an experimental approach to investigate the effects of four independent printing parameters-printing temperature, printing speed, infill type, and layer height-on the tensile mechanical properties of TPU, namely tensile strength, elongation at break, and secant modulus at 100% strain. These output parameters are selected because TPU is a unique thermoplastic elastomer often described as a "bridge between rubber and plastic." While TPU exhibits rubber-like elasticity, it can be processed using conventional thermoplastic methods, making it fundamentally different from rigid polymers such as PLA or PETG. In accordance with ASTM D412, the secant modulus at 100% strain is reported to characterize material stiffness.

Due to this combination of high elasticity and high abrasion resistance, TPU is widely used in applications ranging from footwear and ski boots to gaskets, conduits, and sealing components [24]. Understanding how FDM printing parameters influence its mechanical behavior is therefore essential for both functional design and process optimization. The overall experimental sequence adopted in this study is illustrated in Figure 1, which presents the experimental workflow based on the Taguchi method.

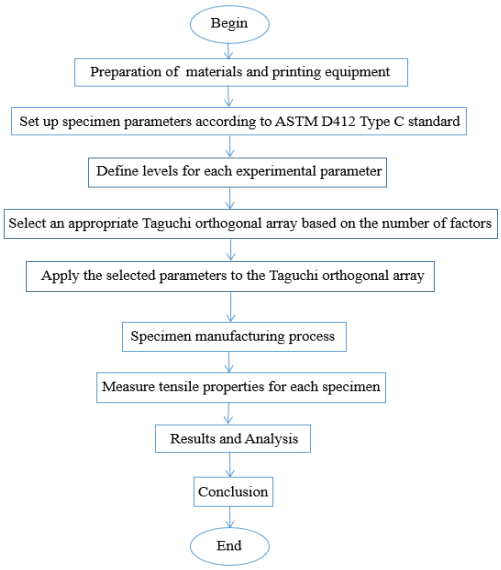

Figure 1. Experimental workflow based on the Taguchi method for evaluating the effects of fused deposition modeling (FDM) printing parameters on the tensile properties of thermoplastic polyurethane (TPU)

2.1 Printing material

The material used in this study is TPU-95A filament supplied by Van Vat Ket Noi Technology Co., Ltd. All tensile specimens were fabricated using this material. The key physical and processing characteristics of the TPU filament, as provided by the manufacturer, are summarized in Table 1.

2.2 Test specimen design

All tensile test specimens were printed using a Bambu Lab P1S FDM 3D printer and designed in accordance with the ASTM D412-16 standard for elastomeric materials [25]. A dumbbell-shaped specimen (Type C) was selected for tensile testing.

The specimen geometry was designed using AutoCAD, and the standardized shape is illustrated in Figure 2. The detailed dimensions of the specimens are listed in Table 2.

Table 1. Manufacturer-specified physical and processing properties of TPU-95A filament used in this study

Performance	Parameter	Unit
Plastic fiber diameter	1.75	mm
Printing temperature	190-230	℃
Printing speed	30-60	mm/s
Heating plate temperature	≈ 40	℃
Density	1.25 ± 0.05	g/cm³
Hardness	95	Shore A
Tolerance	± 0.05	mm

Note: TPU = thermoplastic polyurethane

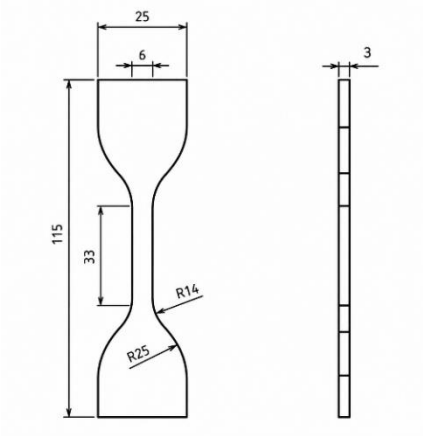

Figure 2. Geometry of ASTM D412 Type C dumbbell-shaped tensile specimen

Table 2. Geometric dimensions of ASTM D412 Type C tensile test specimens

Dimensions	Value (mm)
Total length	115
Tail width	25
Length of the measurement	33
Measurement range width	6
Outer circle diameter	14
Diameter of the rounded circle	25
Sample thickness	3 ± 0.3

2.3 Set parameters for experiment

In this study, the printing parameters are classified into variable parameters and fixed parameters. The variable parameters are selected based on previous studies and include printing temperature, printing speed, layer height, and infill type [22, 26, 27]. These parameters are expected to directly influence interlayer bonding, filament orientation, and internal structure, which in turn affect tensile behavior.

Fixed parameters are adopted from the default material settings in Bambu Studio software and are maintained constant for all experiments to isolate the effects of the selected variables. The ranges and levels of the variable parameters are listed in Table 3, while the fixed parameters are summarized in Table 4. The sample placement angle was set to 45° to capture a balanced anisotropic response of FDM-fabricated specimens. Unlike 0° and 90° orientations, which represent filament-dominated and interlayer-dominated behavior, respectively, the 45° configuration provides a combined

loading condition that is more representative of practical service scenarios.

Table 3. Control factors and corresponding levels for the Taguchi experimental design

No.	Factor	Symbol		Value Level			Range of Change
		Nature	Encryption	Below, -1	Facility, 0	Above, +1	
1	Printing temperature	t	x_1	210	220	230	20
2	Printing speed	v	x_2	20	40	60	20
3	Class height	h	x_3	0.12	0.16	0.2	0.04
4	Infill type	I	x_4	Grid	Rectilinear	Concentric	-

Note: The symbols x1–x4 represent the coded factors used in the Taguchi experimental design.

Table 4. Fixed printing parameters used for specimen fabrication

Specifications	Parameter	Unit
Infill density	100	%
Extrusion ratio	100	%
Sample placement angle	45	◦
Top/bottom layer thickness	0.8	Mm
Wall thickness	1.2	Mm
Heating plate temperature	60	℃
Print line width	0.4	Mm

Three replicate specimens (n = 3) were fabricated for each parameter combination defined by the Taguchi orthogonal array, and the experimental results are presented as mean ± standard deviation.

2.4 Taguchi method

The Taguchi method, developed by Dr. Genichi Taguchi, is a robust design approach aimed at minimizing quality variation by optimizing process parameters. By employing orthogonal arrays, the Taguchi method significantly reduces the number of experiments required while still capturing the main effects of input parameters on output responses.

The method evaluates performance using the signal-to-noise (S/N) ratio, derived from the loss function:

$$L = k\,(y - m)^2$$

where, y is the measured response, m is the desired value, and k is a constant.

Depending on the optimization objective, three S/N ratio formulations are used:

Higher is better

$$\frac{s}{N} = -10\,log_{10}\left(\frac{1}{n}\sum_{i=1}\frac{1}{y_i^2}\right) \quad (1)$$

Lower is better

$$\frac{s}{N} = -10\,log_{10}\left(\frac{1}{n}\sum_{i=1}y_i^2\right) \quad (2)$$

Assess the impact of factors on nominal is best, then:

$$\frac{s}{N} = 10\,log_{10}\left(\frac{\bar{y}_i^2}{S_i^2}\right) \quad (3)$$

where, $\bar{y} = \frac{1}{n}\sum_{u=1} y_u$

$$s^2 = \frac{1}{n-1}\sum_{u=1}^{n}(y_u - \bar{y})^2 \quad (4)$$

where, n and s are $\bar{y}$ the number of experiments, the standard deviation, and the mean, respectively. In all cases, the larger the S/N ratio, the better the obtained characteristic.

Because it does not utilize all experimental combinations, the Taguchi method cannot provide a precise figure for the influence of a particular input parameter (Factor) on the output result; it only provides guidance. Nevertheless, by evaluating the S/N ratio, technologists can understand the trend and extent of the influence of each technological parameter on the output result. This understanding helps researchers quickly identify the technological parameters and the scope of intervention needed to achieve the best output performance. Based on the assessment of the individual influence of each parameter, the optimal combination of technological parameters for the desired output characteristic can be determined.

Numerous studies and applications since the 1970s have shown that the Taguchi method can be used for academic research, as well as for applications in production, and is particularly suitable for those with limited knowledge of statistics [28].

Table 5. Selection of Taguchi orthogonal array (L_N) based on the number of factors and levels

Number of Value Levels	Number of Factors															
	2	3	4	5	6	7	8	9	10	11	12	13	14	15	16
2	L4	L4	L8	L8	L8	L8	L12	L12	L12	L12	L16	L16	L16	L16	L32
3	L9	L9	L9	L18	L18	L18	L18	L27	L27	L27	L27	L27	L36	L36	L36
4	L16	L16	L16	L16	L32	L32	L32	L32	L32						
5	L25	L25	L25	L25	L25	L50	L50	L50	L50	L50	L50				

Table 6. Taguchi L9 orthogonal array with assigned printing parameters for experimental runs

No.	Factors				Printing Parameters			
	x_1	x_2	x_3	x_4	Printing Temperature (°C)	Printing Speed (mm/s)	Layer Height (mm)	Infill Type
1	1	1	1	1	210	20	0.12	Grid
2	1	2	2	2	210	40	0.16	Rectilinear
3	1	3	3	3	210	60	0.20	Concentric
4	2	1	2	3	220	20	0.16	Concentric
5	2	2	3	1	220	40	0.20	Grid
6	2	3	1	2	220	60	0.12	Rectilinear
7	3	1	3	2	230	20	0.20	Rectilinear
8	3	2	1	3	230	40	0.12	Concentric
9	3	3	2	1	230	60	0.16	Grid

Note: The symbols x1–x4 represent the coded factors used in the Taguchi experimental design.

Since the problem has 4 factors and each factor has 3 values, we choose L9 from in Table 5, and our goal is to optimize tensile strength, so we will choose the goal as "Higher is better". After selecting the orthogonal matrix, we need to use it to test the elements. We will assign the test print parameters to matrix L9, as shown in Table 6.

2.5 Specimens manufacturing process

The specimen manufacturing process begins with the design of the tensile test geometry in Autodesk AutoCAD 2025. The model is then imported into Bambu Studio software, where the printing parameters-layer height, printing speed, extrusion temperature, and infill type are configured according to the experimental matrix in Table 6. The slicing configuration and toolpath preparation of the tensile specimen prior to fabrication are illustrated in Figure 3.

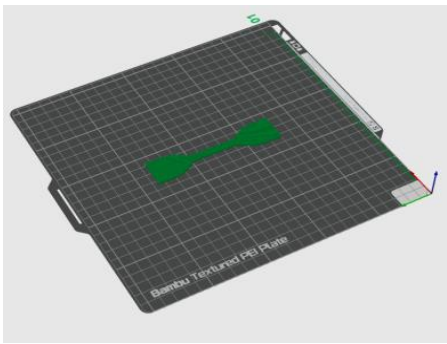

Figure 3. Slicing configuration of the ASTM D412 Type C specimen using Bambu Studio prior to fused deposition modeling (FDM) printing

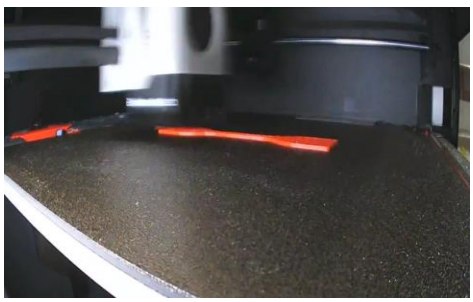

Figure 4. Fused deposition modeling (FDM) printing process of the thermoplastic polyurethane (TPU) tensile specimen using the Bambu Lab P1S printer

Prior to printing, the TPU filament is loaded into the printer, and the extruder is heated to the designated temperature. The finalized model is converted into G-code format, with each parameter combination saved as a separate, numbered file on an SD card. The corresponding file is then selected on the Bambu Lab P1S printer, and the specimen is fabricated. After printing, each specimen is carefully removed, labeled, and prepared for subsequent mechanical testing. The fabrication process of the TPU tensile specimens using the Bambu Lab P1S printer is illustrated in Figure 4. Photographs of the printed specimens after fabrication are presented in Figure 5.

Figure 5. Post-printing images of fabricated specimens

3. RESULTS AND ANALYSIS

3.1 Results

The printed specimens were subjected to tensile testing using a Tensilon universal testing machine with a 100 kgf load capacity, in accordance with ASTM D412. Dumbbell-shaped specimens were mounted in the machine grips and carefully aligned symmetrically to ensure uniform distribution of tensile stress across the cross-section, thereby minimizing bending effects and ensuring accurate determination of maximum tensile strength.

Figure 6. Specimen setup for tensile testing prior to loading

Unless otherwise specified, the crosshead speed was maintained at 500 ± 50 mm/min (20 ± 2 in./min). The test was initiated, and the distance between the gauge marks was continuously monitored while avoiding parallax errors. The applied force was recorded at the specified elongation and at the point of fracture. Tensile stress, tensile strength, and yield point were determined from the recorded force-elongation data. The specimen was mounted and aligned in the testing grips prior to loading, as shown in Figure 6.

Elongation was measured using an elongation-measuring device or a self-recording mechanism. At the moment of fracture, the elongation was recorded to the nearest 10%, as specified in the standard.

Figure 7. Post-test image of the specimen after uniaxial tensile deformation

Figure 8. Fractured specimens after tensile testing

Tensile strain was evaluated by clamping the specimen symmetrically and applying tension smoothly until the specified elongation was reached within 15 seconds. The specimen was held at this elongation for 10 minutes, after which the load was released rapidly without allowing the specimen to retract. The specimen was then allowed to rest for 10 minutes, after which the distance between the reference gauge marks was measured with an accuracy of ± 1% of the original gauge length. A stopwatch was used to ensure precise timing throughout the procedure. The specimen after stretching is shown in Figure 7. As shown in Figure 8, the specimens exhibit distinct fracture patterns following tensile loading.

From the obtained parameters, the stress-strain curve (Figure 9) is used to determine the fracture point. The tensile properties are calculated according to the ASTM D412 standard. Tensile strength:

$$TS = {}^{F_{max}}/_{A}$$

where, F_{max} is the maximum force at the fracture point, and A is the original cross-sectional area of the specimen. Elongation at break:

$$E = \left({}^{L - L_0}/_{L_0}\right) \times 100;$$

where, L is the gauge length at fracture, and L_0 is the initial gauge length. Secant modulus at 100% strain (modulus at 100% elongation):

$$E_{100} = {}^{\sigma_{100}}/_{\varepsilon_{100}};$$

where, σ_{100} is the engineering stress at 100% strain, and $\varepsilon_{100} = 1$ (corresponding to 100% strain).

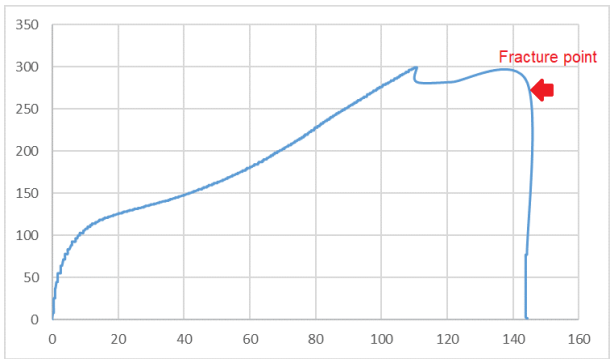

Figure 9. Representative engineering stress−strain curve for specimen 1 (Printing parameters: 210 °C, 20 mm/s, 0.12)

Table 7. Tensile properties of the printed samples under different printing parameter combinations

No.	Factors				Elongation	Tensile Strength	Secant Modulus at 100% Strain	n
	x_1	x_2	x_3	x_4	%	MPa	MPa	
1	1	1	1	1	342.8 ± 6.8	17.5 ± 0.4	9.5 ± 0.2	3
2	1	2	2	2	358.7 ± 7.2	21.1 ± 0.5	11.1 ± 0.3	3
3	1	3	3	3	230.8 ± 5.5	15.4 ± 0.3	10.2 ± 0.2	3
4	2	1	2	3	248.0 ± 6.0	15.6 ± 0.3	9.9 ± 0.2	3
5	2	2	3	1	370.7 ± 8.1	17.9 ± 0.4	8.9 ± 0.2	3
6	2	3	1	2	430.3 ± 9.5	16.7 ± 0.4	9.3 ± 0.3	3
7	3	1	3	2	296.8 ± 6.7	12.5 ± 0.3	8.3 ± 0.3	3
8	3	2	1	3	268.3 ± 6.2	12.5 ± 0.3	8.2 ± 0.2	3
9	3	3	2	1	901.1 ± 18.5	17.5 ± 0.5	8.3 ± 0.3	3

Note: The symbols x1–x4 represent the coded factors used in the Taguchi experimental design.

After recording the results, an overall assessment of samples 1 to 9 showed stable tensile strength from 210 to 350 (12-21 MPa). Samples 1, 2, 5, 6, and 9 achieved elongation at break greater than 300%, elastic modulus greater than 12 MPa, and increased steadily with elongation from 100% to 300%, consistent with elastomer (rubber) in terms of elongation at break. They exhibited higher hardness than conventional rubber while retaining flexibility, with good elasticity and similar properties to TPV.

From Table 7, Sample 2 exhibits the highest tensile strength and secant modulus at 100% strain, reaching 21.1 ± 0.5 MPa and 11.1 ± 0.3 MPa, respectively. These results were obtained with a printing temperature of 210 ℃, a printing speed of 40 mm/s, a layer height of 0.16 mm, and a rectilinear infill pattern. Sample 9 achieved the highest elongation value of 901.1 ± 18.5% using the following parameters: printing temperature of 230 ℃, printing speed of 60 mm/s, layer height of 0.16 mm, and infill type: Grid.

Group 8 had the lowest secant modulus at 100% strain value of 8.2 ± 0.2 MPa using the following parameters: printing temperature of 230 ℃, printing speed of 40 mm/s, layer height of 0.1 mm, and infill type: Concentric. Sample 8 has the lowest tensile strength value at 12.5 ± 0.3 MPa, using the following parameters: printing temperature of 230 ℃, printing speed of 20 mm/s, layer height of 0.2 mm, and infill type: Rectilinear.

Sample 3 has the lowest elongation value with an elongation ratio of 230.5 ± 5.5%, using the following parameters: printing temperature of 210 ℃, printing speed of 60 mm/s, layer height of 0.2 mm, and infill type: Concentric. Samples 7 and 8 have similar tensile strength and secant modulus at 100% strain values.

The lowest values for tensile strength and secant modulus at 100% strain are 12.5 ± 0.3 MPa and 8.2 ± 0.2 MPa, respectively. Models 7 and 8 also have elongation values between 250% and 300%. Although the output parameters have nearly identical output values, their input values are only the same at a print head temperature of 230 ℃.

Models 3 and 4 are similar, with output parameters such as elongation of 230.8 ± 5.5% and 248.0 ± 6.0%, the lowest among the elongation values, and tensile strength values of 15.4 ± 0.3 MPa and 15.6 ± 0.3 MPa, respectively, and secant modulus at 100% strain values between 10.2 MPa and 9.9 MPa. Although they have similar output values, only one input value is the Infill Type: Concentric.

Models 7, 8, and 9 have the lowest secant modulus at 100% strain values, with values of 8.3 ± 0.3 MPa, 8.2 ± 0.2 MPa, and 8.3 ± 0.3 MPa, respectively. All three samples were printed at an extrusion temperature of 230 ℃, which is lower than that used for samples exhibiting higher modulus values.

Samples with the lowest elongation ratios, such as samples 3, 4, and 8 (230.8 ± 5.5%, 248.0 ± 6.0%, and 268.3 ± 6.2%), share the same input parameter: Concentric infill type. Samples with high tensile strength values (17.5 MPa to 17.9 MPa), such as samples 1, 5, and 9, share the same input parameter: Grid infill type.

Samples with the highest secant modulus at 100% strain values, such as samples 1, 2, and 3 (9.5 ± 0.2 MPa, 11.1 ± 0.3 MPa, and 10.2 ± 0.2 MPa, respectively), all have an input temperature of 210 ℃. compared to samples with higher input printing temperature parameters. Samples with a high elastic modulus generally exhibit stiffer properties.

3.2 Taguchi analysis

3.2.1 Taguchi analysis for tensile strength

As shown in Table 8 and Figure 10, we can assess that printing temperature plays the biggest role in tensile strength properties, followed by infill type, layer height, and printing speed. Looking at the S/N ratio chart, we can see that as temperature increases, tensile strength decreases, similar to the study on ABS plastic where increasing temperature leads to decreased tensile strength. Regarding printing speed, when the printing speed increases to a fixed level such as 40 mm/s, the tensile strength begins to decrease gradually. Similarly, with layer height, increasing the layer height to 0.16 mm also causes the tensile strength of the sample to gradually decrease. As for the infill type, it decreases gradually from Grid to Rectilinear and then Concentric. From the S/N ratios of the parameters as analyzed, we can derive the optimal parameters for the tensile strength of the sample: Printing temperature of 210 ℃, Printing speed of 40 mm/s. The layer height is 0.16 mm and the infill type is Grid, with predicted tensile strength and S/N ratio of 21.9234 MPa and 27.097, respectively, as shown in Table 9.

Table 8. S/N ratio response analysis for tensile strength based on printing parameters

Level	Printing Temperature	Printing Speed	Layer Height	Infill Pattern
1	25.0	23.6	23.8	24.9
2	24.5	24.5	25.1	24.3
3	22.9	24.4	23.6	23.2
Delta	2.1	0.9	1.5	1.7
Rank	1.0	4.0	3.0	2.0

Table 9. Optimal printing parameters and predicted tensile strength

Factor	Printing Temperature	Printing Speed	Class Height	Infill Type	Predicted Tensile Strength
Value	210 (℃)	40 (mm/s)	0.16 (mm)	Grid	21.9234 (MPa)

Table 10. S/N ratio response for elongation under different printing parameters

Level	Printing Temperature	Printing Speed	Layer Height
1	49.69	49.35	50.65
2	50.65	50.35	52.69
3	52.37	53.01	49.37
Delta	2.68	3.67	3.33
Rank	4.00	2.00	3.00

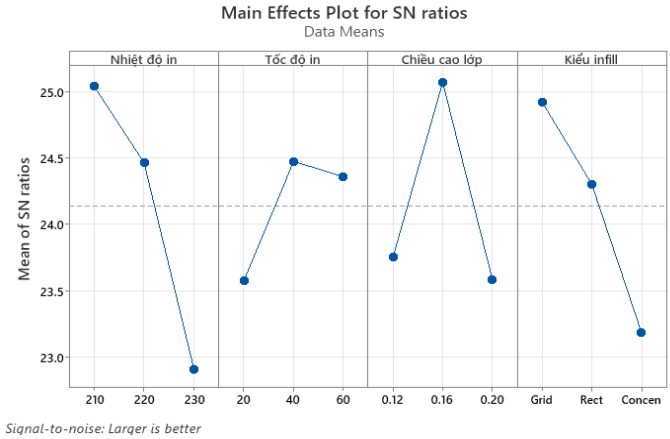

Figure 10. Taguchi S/N ratio analysis for tensile strength optimization

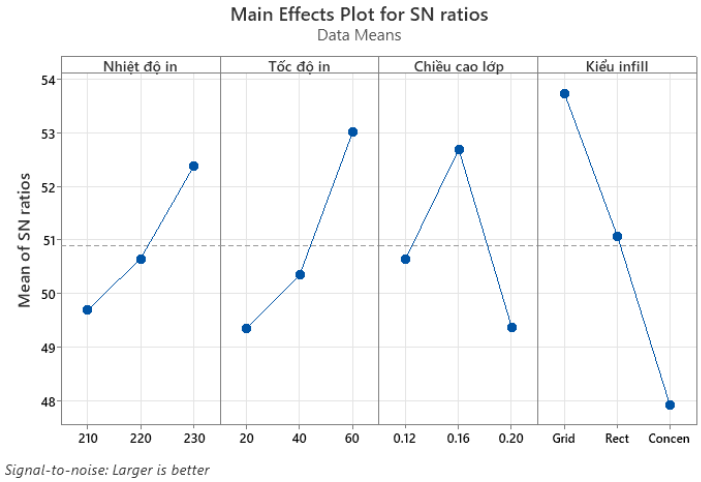

Figure 11. Main effects of printing parameters on elongation using S/N ratio analysis

Figure 12. Main effects of printing parameters on secant modulus using S/N ratio analysis

3.2.2 Taguchi analysis for elongation

From Table 10 and the S/N ratio chart for elongation in Figure 11, the factor with the greatest influence on elongation is the infill type, followed by printing speed, layer height, and printing temperature. We can assess that as printing temperature increases, elongation increases steadily. Printing speed is similar to printing temperature, increasing gradually with increasing speed. For layer height, when increasing the layer height by 0.16 mm, the elongation increases to that level and then gradually decreases. The influence of infill type on elongation is similar to tensile strength, with elongation decreasing gradually from Grid to Rectilinear and Concentric. The input parameters for elongation in the S/N results achieved the highest value in the parameter set in Sample 9, with an elongation of 901.09% with printing parameters of printing temperature of 230 °C, printing speed of 60 mm/s, layer height of 0.16 mm, and infill type of Grid, so no further analysis is needed. Provide the optimal set of parameters for elongation.

3.2.3 Taguchi analysis for secant modulus

Analysis of Table 11 and the S/N ratio plot in Figure 12 indicates that printing temperature has the most significant influence on the secant modulus, followed by layer height, infill type, and printing speed. Similar to the effect on tensile strength, the higher the printing temperature, the lower the secant modulus. Printing speed and layer height increase to a certain level, such as 40 mm/s and 0.16 mm, then decrease gradually. Rectilinear infill achieves the largest Secant modulus, followed by concentric and grid infill. Similar to elongation, the optimal parameters for the secant modulus value are also found in the orthogonal matrix in Sample 2, with a value of 11.099188 MPa, with the parameters being a printing temperature of 210 ℃, a printing speed of 40 mm/s, a layer height of 0.16 mm, and the type of infill. Since the infill is rectilinear, we no longer need an optimization parameter set for this feedback variable.

Table 11. S/N ratio response for secant modulus under different printing parameters

Level	Printing Temperature	Printing Speed	Layer Height
1	20.20	19.28	19.07
2	19.41	19.41	19.71
3	18.35	19.27	19.17
Delta	1.85	0.13	0.64
Rank	1.00	4.00	2.00

Table 12. Regression equations for elongation under different infill patterns

	Infill Pattern
Grid	Elongation = -1549 + 8.90 Printing temperature + 5.62 Printing speed - 596 Layer height
Rect	Elongation = -1725 + 8.90 Printing temperature + 5.62 Printing speed - 596 Layer height
Concen	Elongation = -1838 + 8.90 Printing temperature + 5.62 Printing speed - 596 Layer height

Table 13. Statistical summary of the regression model for elongation

S	R-sq	R-sq (Adj)	R-sq (Pred)
164.10	75.89%	35.70%	0.00%

Note: S denotes the standard error of the regression model. R-sq (coefficient of determination) represents the percentage of response variation explained by the model. R-sq (Adj) is the adjusted coefficient of determination that accounts for the number of predictors in the model. R-sq (Pred) indicates the predictive capability of the model for new observations.

Table 14. Analysis of variance (ANOVA) for the regression model of elongation

Source	DF	Adj SS	Adj MS	F-Value
Regression	5	254219	50844	1.89
Printing temperature	1	47489	47489	1.76
Printing speed	1	75862	75862	2.82
Layer height	1	3411	3411	0.13
Infill pattern	2	127458	63729	2.37
Error	3	80781	26927	-
Total	8	335000	-	-

Note: DF = Degrees of freedom; Adj SS = Adjusted sum of squares; Adj MS = Adjusted mean square; F-Value = Ratio of factor mean square to error mean square used to assess statistical significance

3.3 Analysis of variance analysis

3.3.1 ANOVA analysis for elongation

The goal of ANOVA is to compare the means of multiple groups (populations) based on the means of observed samples from these groups, and through hypothesis testing, to conclude on the equality of these population means. In research, ANOVA is used as a tool to examine the influence of a causal factor (qualitative) on an outcome factor (quantitative). The regression equations for elongation under different infill patterns are presented in Table 12.

Based on the parameters given in Table 13, all input parameters have values greater than 0.05 and are not statistically significant for elongation. The R^2 value of 75.89% indicates that the input parameters explain 75.89% of the variation in elongation. Based on the regression model analysis table in Table 14, we observe that the infill type has the greatest impact on elongation, accounting for 38% of the factors, followed by printing speed with an impact of 22.5%, printing temperature with an impact of 14.2%, and the lowest impact is layer height with an impact of 1%. The p-value used as the significance level is 0.05. ANOVA was performed to analyze tensile strength.

Table 15. Regression equations for tensile strength under different infill patterns

	Infill Pattern
Grid	Tensile strength = 59.4 − 0.1931 Printing temperature + 0.0325 Printing speed − 3.9 Layer height
Rect	Tensile strength = 58.6 − 0.1931 Printing temperature + 0.0325 Printing speed − 3.9 Layer height
Concen	Tensile strength = 56.3 − 0.1931 Printing temperature + 0.0325 Printing speed − 3.9 Layer height

The regression equations for tensile strength under different infill patterns are presented in Table 15. The R^2 value of 69.43%, as shown in Table 16, indicates that the input parameters explain 69.43% of the variation in elongation, which is lower than the elongation itself. Based on the

parameters, the input parameters all have values greater than 0.05 and are not statistically significant for tensile strength. Although input parameters such as printing temperature and infill type are not statistically significant, they still play an important role in improving tensile strength.

Table 16. Statistical summary of the regression model for tensile strength

S	R-sq	R-sq (Adj)	R-sq (Pred)
2.44	69.43%	18.47%	0.00%

Based on the regression model analysis table in Table 17, we find that printing temperature is the factor with the greatest impact on tensile strength, accounting for 38.2% of the factors. Second is the infill type with 26.65%, followed by printing speed with 4.33%, and the lowest is layer height with 0.24%.

Table 17. Analysis of variance (ANOVA) for the regression model of tensile strength

Source	DF	Adj SS	Adj MS	F-Value	P-Value
Regression	5	40.68	8.14	1.36	0.43
Printing temperature	1	22.38	22.38	3.75	0.15
Printing speed	1	2.54	2.54	0.43	0.56
Layer height	1	0.15	0.15	0.02	0.89
Infill pattern	2	15.61	7.81	1.31	0.39
Error	3	17.91	5.97	-	-
Total	8	58.59	-	-	-

Note: DF = Degrees of freedom; Adj SS = Adjusted sum of squares; Adj MS = Adjusted mean square; F-Value = Ratio of factor mean square to error mean square used to assess statistical significance

3.3.2 ANOVA analysis for secant modulus

The regression equations for secant modulus under different infill patterns are presented in Table 18. The R^2 value of 86.93% shown in Table 19 indicates that the input parameters in the regression explain 86.93% of the variation in secant modulus, making this the model with the highest reliability among the models developed.

Table 18. Regression equations for secant modulus under different infill patterns

Infill Pattern	
Grid	Secant modulus = 30.52 − 0.0994 Printing temperature − 0.0001 Printing speed + Layer height
Rect	Secant modulus = 31.19 − 0.0994 Printing temperature − 0.0001 Printing speed + Layer height
Concen	Secant modulus = 31.07 − 0.0994 Printing temperature − 0.0001 Printing speed + Layer height

Table 19. Statistical summary of the regression model for secant modulus

S	R-sq	R-sq (Adj)	R-sq (Pred)
0.58	86.93%	65.15%	0.00%

Based on the regression model analysis table in Table 20, we find that printing temperature is the factor with the greatest impact on tensile strength, accounting for 76.5% of the input factors. The infill type is second with an impact of 9.96%, followed by printing speed with an impact of 2.58%, and the lowest impact is layer height with approximately 0%. Based on the parameters, the p-value for printing temperature is 0.025 and statistically significant for the secant modulus at 100% strain. Therefore, to improve the secant modulus at 100% strain, we only need to adjust the printing temperature.

Table 20. Analysis of variance (ANOVA) for the regression model of secant modulus

Source	DF	Adj SS	Adj MS	F-Value	P-Value
Regression	5	6.72	1.34	3.99	0.14
Printing temperature	1	5.93	5.93	17.6	0.03
Printing speed	1	0.00001	0.00001	0.00	0.10
Layer height	1	0.02	0.02	0.07	0.82
Infill pattern	2	0.78	0.39	1.14	0.43
Error	3	1.01	0.34	-	-
Total	8	7.73	-	-	-

Note: DF = Degrees of freedom; Adj SS = Adjusted sum of squares; Adj MS = Adjusted mean square; F-Value = Ratio of factor mean square to error mean square used to assess statistical significance

It should be noted that the Taguchi ranking and ANOVA results are based on different evaluation criteria. The Taguchi method identifies influential factors through the range of S/N responses, whereas ANOVA assesses statistical significance based on variance relative to experimental error. Consequently, a factor such as printing temperature may exhibit the strongest influence in S/N analysis but remain statistically insignificant ($p > 0.05$) due to limited sample size and experimental variability.

4. SCANNING ELECTRON MICROSCOPY ANALYSIS

SEM was conducted to examine the fracture surface morphology of selected TPU specimens to correlate microstructural features with the mechanical behavior obtained from Taguchi optimization and ANOVA analyses. In this section, Sample 2 and Sample 7 are analyzed and compared, as they represent distinct mechanical responses resulting from different printing parameter combinations.

4.1 Scanning electron microscopy analysis of Sample 2

Sample 2, which exhibited the highest secant modulus (11.10 MPa) and relatively high tensile strength, was printed using a rectilinear infill pattern, a printing temperature of 210 ℃, a printing speed of 40 mm/s, and a layer height of 0.16 mm. SEM images at low magnification reveal a well-organized filament architecture, where deposited filaments retain their geometric integrity and align consistently with the loading direction, as presented in Figure 13.

At intermediate magnifications, the fracture surface shows a dense and homogeneous porous structure, with uniformly distributed micro-pores and minimal interlayer gaps. This indicates effective fusion between adjacent filaments and sufficient polymer chain diffusion at the selected printing temperature. The controlled pore size and continuity of the filament network enhance load transfer efficiency, which explains the superior stiffness observed experimentally.

High-magnification images further reveal elongated fibrils, stretched ligaments, and torn filament bridges, confirming a

ductile fracture mechanism. These features indicate that although Sample 2 prioritizes stiffness, it still retains the intrinsic elasticity of TPU. The observed microstructure strongly supports the ANOVA result, which identified printing temperature as the most influential factor on the secant modulus, contributing approximately 76.5% to the overall variation.

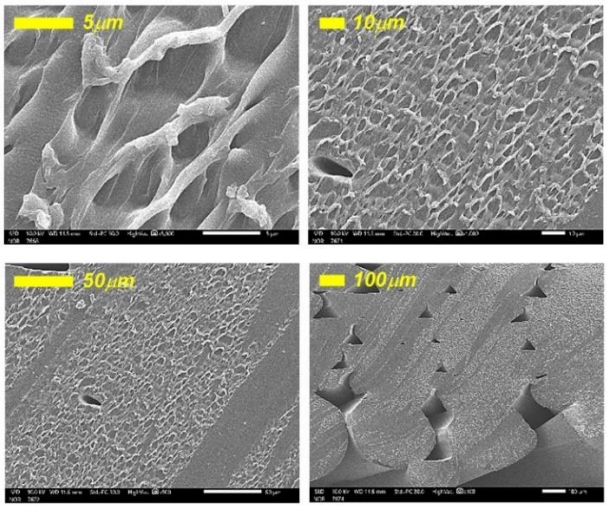

Figure 13. Scanning electron microscopy (SEM) images of Sample 2 at different magnifications, illustrating filament architecture, pore structure, and fracture morphology

4.2 Scanning electron microscopy analysis of Sample 7

Sample 7 exhibits a markedly different fracture morphology compared to Sample 2. At high magnification (×5000), the fracture surface of Sample 7 appears smoother and more planar, with elongated flow lines and fewer fibrillated structures. The presence of localized spherical features and smoother regions suggests reduced interlayer bonding and limited plastic deformation prior to fracture, as illustrated in Figure 14.

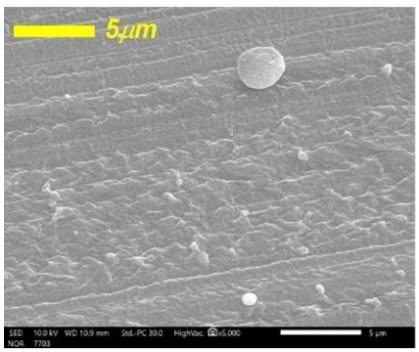

Figure 14. High-magnification scanning electron microscopy (SEM) image of Sample 7 showing smooth fracture surface and limited fibrillation features

Unlike Sample 2, Sample 7 shows fewer filament bridges and less evidence of polymer chain stretching. This indicates that failure occurred more readily along interlayer boundaries, implying weaker adhesion between deposited layers. Such microstructural characteristics are typically associated with lower stiffness and reduced tensile performance, which is consistent with the mechanical results observed for Sample 7.

The relatively smooth fracture surface also suggests that the material experienced less energy absorption during tensile loading, leading to premature crack propagation. This behavior aligns with Taguchi and ANOVA findings, where suboptimal combinations of printing temperature, infill pattern, or printing speed resulted in inferior mechanical properties.

4.3 Comparative microstructural discussion

A direct comparison between Samples 2 and 7 highlights the critical role of printing parameters in defining fracture behavior and mechanical performance. Sample 2 exhibits a rough, fibrillated, and highly interconnected microstructure, indicative of strong interlayer adhesion and effective stress redistribution. In contrast, Sample 7 displays a smoother fracture surface with limited fibrillation, reflecting weaker bonding and reduced resistance to deformation.

These differences can be directly linked to the statistical analyses. The rectilinear infill pattern and optimized printing temperature used in Sample 2 promote filament alignment and polymer diffusion, resulting in higher stiffness and improved tensile behavior. Conversely, the microstructure of Sample 7 confirms the detrimental effect of less favorable parameter combinations, particularly in terms of interlayer bonding quality.

4.4 Correlation with Taguchi and analysis of variance results

The SEM observations provide strong physical validation for the Taguchi and ANOVA analyses. The dominance of printing temperature in influencing the secant modulus is clearly reflected in the enhanced filament fusion and reduced interfacial defects observed in Sample 2. Similarly, the reduced deformation mechanisms observed in Sample 7 explain its lower mechanical performance.

Furthermore, the contrast between the two samples demonstrates that microstructural integrity and fracture morphology are reliable indicators of mechanical behavior in FDM-printed TPU. The consistency between experimental results, statistical modeling, and SEM evidence confirms the robustness of the optimization methodology used in this study.

In summary, SEM analysis reveals that:

- Sample 2 achieves superior mechanical performance due to strong interlayer bonding, controlled pore morphology, and ductile fracture behavior.
- Sample 7 exhibits smoother fracture surfaces and reduced fibrillation, indicating weaker interlayer adhesion and lower energy absorption.
- Microstructural differences observed by SEM directly correspond to trends identified through Taguchi optimization and ANOVA.

These findings confirm that optimized printing parameters significantly enhance microstructural quality, which in turn governs the mechanical performance of TPU components fabricated using FDM technology.

4.5 Mechanistic interpretation

The mechanical differences between Samples 2 and 7 can be explained by the phase-separated structure of TPU, consisting of soft segments and hard domains (microphase separation).

At the optimal printing temperature (210 ℃, Sample 2), increased soft-segment mobility enhances polymer chain interdiffusion and entanglement across layers (polymer chain reptation), resulting in strong interlayer bonding and dense filament fusion. Meanwhile, partial disruption and reformation of hard-segment hydrogen bonds preserve domain integrity, contributing to higher stiffness and modulus.

In contrast, suboptimal conditions in Sample 7 limit chain mobility and interlayer diffusion, leading to weak adhesion and interfacial failure. The smoother fracture surface and reduced fibrillation indicate limited plastic deformation and lower energy absorption.

Overall, printing temperature governs molecular mobility and hard-domain organization, directly controlling interlayer bonding quality and macroscopic mechanical performance.

5. CONCLUSIONS

This study systematically investigated the effects of key FDM processing parameters on the tensile behavior of TPU by integrating Taguchi design, ANOVA, mechanical testing, and SEM analysis.

- Printing temperature is the primary governing factor across all responses, especially stiffness, highlighting the critical role of interlayer diffusion and bonding in determining mechanical integrity.
- Infill type strongly influences elongation and energy absorption, indicating that mechanical response in TPU is highly sensitive to mesoscale structural design.
- The combined statistical and microstructural analyses demonstrate that optimized processing conditions enhance filament fusion and fracture morphology, leading to improved stress transfer and ductility.

The findings are based on a limited Taguchi design and a single TPU material system, which may constrain generalizability. Future studies should extend validation across broader processing windows, different TPU grades, and more complex geometries, as well as incorporate fully quantitative microstructural characterization to strengthen process-structure-property relationships.

The present study should be regarded as a screening-level investigation aimed at identifying relative parameter effects rather than providing statistically rigorous property evaluation. The observed trends are consistent with findings reported in the literature, which supports the qualitative validity of the identified parameter influences. The findings of this study provide preliminary insights into the influence of FDM process parameters.

Future work will focus on improving the statistical robustness of the findings by incorporating multiple replicates for each parameter combination.

ACKNOWLEDGEMENT

This work was financially supported by Ho Chi Minh City University of Industry and Trade under Contract No. 132/HĐ-DCT dated 15 July 2024.

REFERENCES

[1] Xiao, J.H., Gao, Y.F. (2017). The manufacture of 3D printing of medical grade TPU. Progress in Additive Manufacturing, 2(3): 117-123. https://doi.org/10.1007/s40964-017-0023-1

[2] Daminabo, S.C., Goel, S., Grammatikos, S.A., Nezhad, H.Y., Thakur, V.K. (2020). Fused deposition modeling-based additive manufacturing (3D printing): Techniques for polymer material systems. Materials Today Chemistry, 16: 100248. https://doi.org/10.1016/j.mtchem.2020.100248

[3] Risad, R.H., Ahmed, M.H., Basher, A., Rashid, S., Shishir, M.M.A., Hossain, K.R. (2024). FDM printing process and its biomedical application. Chemical Research and Technology, 1(3): 138-149. https://doi.org/10.22034/chemrestec.2024.467346.1021

[4] Chen, H., Yang, X., Chen, L.T., Wang, Y., Sun, Y.C. (2016). Application of FDM three-dimensional printing technology in the digital manufacture of custom edentulous mandible trays. Scientific Reports, 6(1): 19207. https://doi.org/10.1038/srep19207

[5] Sanchez Ramirez, A., Islán Marcos, M.E., Blaya Haro, F., D'Amato, R., Sant, R., Porras, J. (2019). Application of FDM technology to reduce aerodynamic drag. Rapid Prototyping Journal, 25(4): 781-791. https://doi.org/10.1108/RPJ-09-2018-0251

[6] Zagidullin, R.S., Zezin, N.I., Rodionov, N.V. (2021). Improving the quality of FDM 3D printing of UAV and aircraft parts and assemblies by parametric software changes. IOP Conference Series: Materials Science and Engineering, 1027: 012031. https://doi.org/10.1088/1757-899X/1027/1/012031

[7] Novak-Marcincin, J., Novakova-Marcincinova, L., Barna, J., Janak, M. (2012). Application of FDM rapid prototyping technology in experimental gearbox development process. Tehnički Vjesnik, 19(3): 689-694.

[8] Wu, P., Wang, J., Wang, X.Y. (2016). A critical review of the use of 3-D printing in the construction industry. Automation in Construction, 68: 21-31. https://doi.org/10.1016/j.autcon.2016.04.005

[9] Camacho, D.D., Clayton, P., O'Brien, W.J., Seepersad, C., Juenger, M., Ferron, R., Salamone, S. (2018). Applications of additive manufacturing in the construction industry-A forward-looking review. Automation in Construction, 89: 110-119. https://doi.org/10.1016/j.autcon.2017.12.031

[10] Wang, J., Yang, B., Lin, X., Gao, L., Liu, T., Lu, Y.L., Wang, R.G. (2020). Research of TPU materials for 3D printing aiming at non-pneumatic tires by FDM method. Polymers, 12(11): 2492. https://doi.org/10.3390/polym12112492

[11] Gupta, P., Kumar, A. (2024). Comparison of tensile properties of 3D printed PETg and ABS materials, International Journal for Scientific Research Innovations, 2(2): 1-11. https://ijsri.amberpublishers.in/resources/papers/p1%20v2i2.pdf.

[12] Ekşi, S., Karakaya, C. (2025). Effects of process parameters on tensile properties of 3D-printed PLA parts fabricated with the FDM method. Polymers, 17(14): 1934. https://doi.org/10.3390/polym17141934

[13] Sapkota, A., Ghimire, S.K., Adanur, S. (2025). Fused deposition modeling (FDM) process parameter optimization for mechanical properties of 3D-printed woven fabric structures using Taguchi method. Journal of Industrial Textiles, 55: 15280837251339124.

https://doi.org/10.1177/15280837251339124
[14] Trinh, V.L., Hoang, T.D., Ngo, Q.T. (2025). The influence of processing parameters on the tensile strength of 3D printed products. Engineering, Technology Applied Science Research, 15(3): 22663-22668. https://doi.org/10.48084/etasr.10573
[15] Rismalia, M., Hidajat, S.C., Permana, I.G.R., Hadisujoto, B., Muslimin, M., Triawan, F. (2019). Infill pattern and density effects on the tensile properties of 3D printed PLA material. Journal of Physics: Conference Series, 1402(4): 044041. https://doi.org/10.1088/1742-6596/1402/4/044041
[16] Nguyen, T.K., That, N.T.T., Nguyen, B.D. (2024). 3D printing parameters for optimum tensile strength using the taguchi-based response surface method. Multi-Criteria Decision-Making and Optimum Design with Machine Learning, pp. 72-87
[17] Mahameru, R.D.K., Faizin, A.K., Lamura, M.D.P., Lestari, W.D. (2025). Optimization of 3D printing parameters for enhanced pla tensile strength using the taguchi method. International Journal of Automotive and Mechanical Engineering, 22(1): 12035-12047. https://doi.org/10.15282/ijame.22.1.2025.7.0924
[18] Muhamedagic, K., Berus, L., Potočnik, D., Cekic, A., Begic-Hajdarevic, D., Cohodar Husic, M., Ficko, M. (2022). Effect of process parameters on tensile strength of FDM printed carbon fiber reinforced polyamide parts. Applied Sciences, 12(12): 6028. https://doi.org/10.3390/app12126028
[19] Kumaresan, R., Kadirgama, K., Samykano, M., Harun, W.S.W., Thirugnanasambandam, A., Kanny, K. (2025). In-depth study and optimization of process parameters to enhance tensile and compressive strengths of PETG in FDM technology. Journal of Materials Research and Technology, 37: 397-416. https://doi.org/10.1016/j.jmrt.2025.06.013
[20] Wach, R.A., Wolszczak, P., Adamus-Włodarczyk, A. (2018). Enhancement of mechanical properties of FDM-PLA parts via thermal annealing. Macromolecular Materials and Engineering, 303(9): 1800169. https://doi.org/10.1002/mame.201800169
[21] Sukindar, N.A., Rahim, N.A.A.A., Yasir, A.S.H.M., Kamaruddin, S., et al. (2024). Optimization of FDM 3D printing parameters for tensile strength of PETG carbon fibre using Taguchi method. International Journal of Modern Manufacturing Technologies, 16(3): 143-152. https://doi.org/10.54684/ijmmt.2024.16.3.143
[22] Hohimer, C., Christ, J., Aliheidari, N., Mo, C., Ameli, A. (2017). 3D printed thermoplastic polyurethane with isotropic material properties. In SPIE Smart Structures and Materials + Nondestructive Evaluation and Health Monitoring, pp. 213-221. https://doi.org/10.1117/12.2259810
[23] Le, D., Nguyen, C.H., Pham, T.H.N., Nguyen, V.T., Pham, S.M., Le, M.T., Nguyen, T.T. (2023). Optimizing 3D printing process parameters for the tensile strength of thermoplastic polyurethane plastic. Journal of Materials Engineering and Performance, 32(23): 10805-10816. https://doi.org/10.1007/s11665-023-07892-8
[24] Qi, H.J., Boyce, M.C. (2005). Stress-strain behavior of thermoplastic polyurethanes. Mechanics of Materials, 37(8): 817-839. https://doi.org/10.1016/j.mechmat.2004.08.001
[25] ASTM D412-16. (2021). Standard test methods for vulcanized rubber and thermoplastic elastomers—Tension. ASTM International, United States. https://store.astm.org/d0412-16r21.html.
[26] Miazio, Ł. (2019). Impact of print speed on strength of samples printed in FDM technology. Agricultural Engineering, 23(2): 33-38. https://doi.org/10.1515/agriceng-2019-0014
[27] Ulkir, O., Ertugrul, I., Ersoy, S., Yağımlı, B. (2024). The effects of printing temperature on the mechanical properties of 3D-printed acrylonitrile butadiene styrene. Applied Sciences, 14(8): 3376. https://doi.org/10.3390/app14083376
[28] Gulo, T., Mardiyana, D., Sumarno, D.I. (2025). Analysis of print speed variations effect and nozzle temperature on the tensile strength of 3D printed TPU-95A products. Jurnal Konversi Energi dan Manufaktur, 10(1): 53-60. https://doi.org/10.21009/JKEM.10.1.6